

# Organic Field-Effect Transistors

By Gilles Horowitz\*

Organic field-effect transistors (OFETs) were first described in 1987. Their characteristics have undergone spectacular improvements during the last two or three years. At the same time, several models have been developed to rationalize their operating mode. In this review, we examine the performance of OFETs as revealed by recently published data, mainly in terms of field-effect mobility and on-off current ratio. We compare the various compounds that have been used as the active component, and describe the most prominent fabrication techniques. Finally, we analyze the charge transport mechanisms in organic solids, and the resulting models of OFETs.

## 1. Introduction

The principle of the field-effect transistor (FET) was first proposed by Lilienfeld in 1930.<sup>[1]</sup> Basically, a FET operates as a capacitor where one plate is a conducting channel between two ohmic contacts, the source and drain electrodes. The density of charge carriers in the channel is modulated by the voltage applied to the second plate of the capacitor, the gate electrode. It was only in 1960 that Kahng and Atalla<sup>[2]</sup> fabricated the first silicon-based metal-oxide-semiconductor FET (MOSFET). Nowadays, the MOSFET is probably the most prominent constituent of modern microelectronics, both as discrete devices and in integrated circuits. The MOSFET has several acronyms, including MISFET (metal-insulator-semiconductor FET), which will be chiefly used here, and IGFET (insulated gate FET). MOSFETs are mainly fabricated with single-crystalline silicon, because of the excellent quality of the silicon-silicon oxide interface.

Although first descriptions of the field effect in organic semiconductors date back to 1970,<sup>[3-5]</sup> organic FETs (OFETs) have only been identified as potential elements of electronic devices since the report by Koezuka and co-workers, in 1987, on a structure based on electrochemically polymerized polythiophene.<sup>[6]</sup> Polythiophene belongs to the family of conducting (or conjugated) polymers (CPs) that were discovered in the late 1970s. It appeared more recently that small conjugated molecules, the semiconducting properties of which have long been recognized,<sup>[7]</sup> are also promising materials for this application. OFETs adopt the architecture of the thin film transistor (TFT), which has proven its adaptability with low conductivity materials, particularly in the case of amorphous hydrogenated silicon (a-Si:H).<sup>[8]</sup> The performance of OFETs has continuously improved since then, and some OFETs now compete with amorphous silicon FETs, which are now preferred to conventional crystalline silicon FETs in applications where large areas are needed.

Several reviews on OFETs have been published in the past.<sup>[9-11]</sup> In the present paper, I shall concentrate on the present state-of-the-art of OFETs. The various materials and fabrication techniques will be detailed, and their performance compared. A survey of the charge transport mechanisms in organic semiconductors will also be made, and various models developed for the OFETs examined.

## 2. Field-Effect Transistors<sup>[12]</sup>

The structures of three kinds of FET are illustrated in Figure 1. A MISFET (Fig. 1a) consists of a p-type semiconductor on which two n<sup>+</sup> regions have been formed. Two ohmic contacts, the source and the drain, are constructed on these doped regions. The third electrode, the gate, which is used to modulate the conductivity of the source-drain channel, is isolated from the semiconductor substrate by an insulating layer. In the MESFET (Fig. 1b), the n<sup>+</sup> source and drain are grown on an n-type substrate, and a Schottky barrier is used to isolate the gate electrode. Finally, the TFT (Fig. 1c) consists of a thin semiconducting layer equipped with two ohmic contacts and an insulated gate.

### 2.1. The MISFET

#### 2.1.1. Metal-Insulator-Semiconductor Junction

The energy-band diagram of an ideal MIS diode is given in Figure 2 (for a p-type semiconductor). The diode is termed *ideal* because the bands are flat for zero applied voltage. This is the case when Equation 1 is fulfilled.

$$\phi_m - \left( \chi + \frac{E_g}{2q} + \phi_b \right) = 0 \quad (1)$$

Here,  $\phi_m$  is the metal workfunction,  $E_g$  the semiconductor bandgap,  $q$  the absolute electron charge, and  $\phi_b$  the potential difference between the Fermi level and the intrinsic Fermi level  $E_i$  (which is located very close to midgap.) (In the non-ideal case, a small band curvature exists at the in-

[\*] Dr. G. Horowitz  
Laboratoire des Matériaux Moléculaires, CNRS  
2 rue Henry-Dunant, F-94320 Thiais (France)

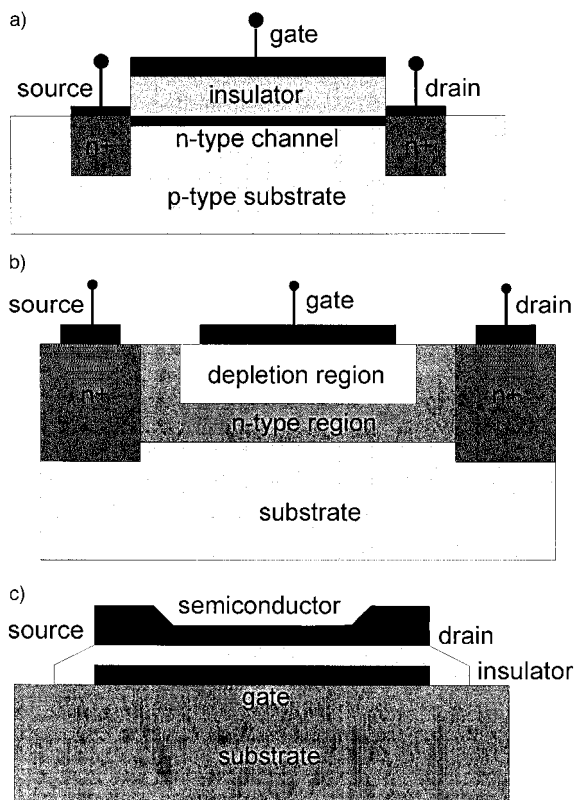


Fig. 1. Schematic views of three kinds of field-effect transistor: a) the metal-insulator-semiconductor FET (MISFET), b) the metal-semiconductor FET (MESFET), and c) the thin film transistor (TFT).

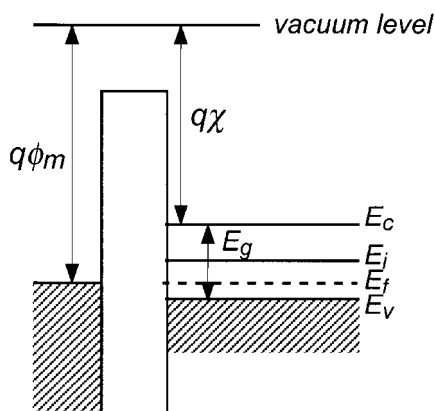


Fig. 2. Band diagram of an ideal metal-insulator-semiconductor structure at equilibrium.



Gilles Horowitz was born in 1949 in Paris. He graduated in solid-state physics from the University of Paris 7 in 1973. He then spent two years at the Centre d'Etude des Télécommunications (CNET) at Lannion, France, working on ion implantation in gallium arsenide. In 1976 he entered the Centre National de la Recherche Scientifique (CNRS), with a post at the Centre d'Etudes Nucleaires at Saclay, near Paris, where he studied the photoelectrochemical conversion and storage of solar energy on semiconductor electrodes. In the meantime, he received his Ph.D. in 1981 at the University of Paris 7. In 1982 he joined the Laboratoire des Matériaux Moléculaires at Thiais. Since 1987, his main interest has lain in the electrical and optical properties of organic semiconductors, which includes the realization of photovoltaic cells, thin film transistors, and light emitting diodes.

insulator–semiconductor interface, and a small potential  $V_{fb}$ , the so-called flat-band voltage, must be applied to the metal to get the flat-band conditions.) When the MIS diode is biased with positive or negative voltages, three different situations may occur at the insulator–semiconductor interface. For a negative voltage (Fig. 3a), the bands bend upward and the top of the valence band moves closer to the Fermi level, causing an *accumulation* of holes near the insulator–semiconductor interface. A *depletion* of majority carriers occurs in the case of a moderate positive voltage (Fig. 3b). When a larger positive voltage is applied to the metal (Fig. 3c), the bands bend even more downward and the intrinsic level eventually crosses the Fermi level. At this point, the density of electrons exceeds that of the holes, and one enters the *inversion* regime.

### 2.1.2. Principles of Operation

In all cases, the source contact will be assumed to be connected to the ground. When a sufficiently high positive voltage is applied to the gate of a MISFET (see Fig. 1a), an inversion layer forms at the insulator–semiconductor interface, providing a conducting channel between the source and the drain. This turns the device on. One of the main advantages of the MISFET structure is that the depletion region between the p-type substrate and both the n-channel and the  $n^+$  regions below the source and drain contacts provides isolation from any other device fabricated on the same substrate. Very low off currents are also achieved because both  $n^+$  regions act as reverse-biased diodes.

The current–voltage characteristics of the MISFET are calculated in the gradual channel (or Shockley) approximation, based on the assumption that the electric charge density related to a variation of the electric field along the channel is much smaller than that related to a variation across the channel, namely  $|\partial F_x/\partial x| \ll |\partial F_y/\partial y|$ , where  $F$  is the electric field, and  $x$  and  $y$  the directions parallel and perpendicular to the insulator–semiconductor interface, respectively. This condition is generally fulfilled when the channel length  $L$  is much larger than the insulator thickness  $d_i$ . If we assume in addition that the charge mobility  $\mu$  is constant, the drain current  $I_d$  is related to the source–drain voltage  $V_d$  and source–gate voltage  $V_g$  through Equation 2.

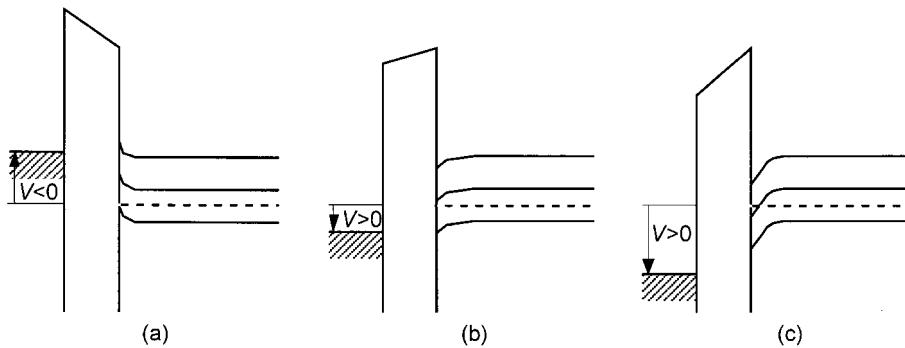


Fig. 3. Same as Figure 2 for a polarized MIS diode, under accumulation (a), depletion (b), and inversion (c) regimes.

$$I_d = \frac{Z}{L} \mu C_i \left\{ \left( V_g - 2\phi_b - \frac{V_d}{2} \right) V_d - \frac{2\sqrt{2\varepsilon_s q N_a}}{C_i} \left[ (V_d + 2\phi_b)^{3/2} - (2\phi_b)^{3/2} \right] \right\} \quad (2)$$

Here,  $Z$  is the channel width,  $C_i$  the insulator capacitance (per unit area),  $\varepsilon_s$  the semiconductor permittivity, and  $N_a$  the doping level of the p-type substrate. Equation 2 predicts that, for a given gate voltage, the drain current first increases linearly with the drain voltage (linear regime), then gradually levels off to a constant value (saturation regime). It also predicts that the drain current increases when the gate voltage increases. A set of drain current–voltage curves for various gate voltages is shown in Figure 4. For a small  $V_d$ , Equation 2 reduces to Equation 3, where  $V_t$ , the threshold voltage, which corresponds to the onset of the strong inversion regime, is given by Equation 4.

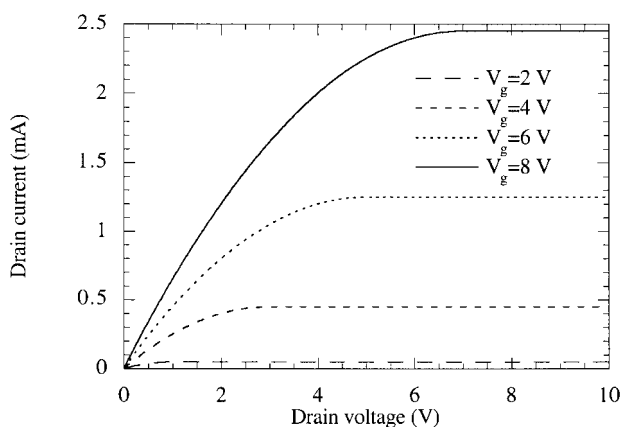


Fig. 4. Current–voltage characteristics of a MISFET for various gate voltages.

$$I_d = \frac{Z}{L} \mu C_i (V_g - V_t) V_d \quad (3)$$

$$V_t = 2\phi_b + \frac{\sqrt{2\varepsilon_s q N_a} (2\phi_b)}{C_i} \quad (4)$$

Two important technological parameters are the channel conductance  $g_d$  and the transconductance  $g_m$ , which, in the

linear regime, are given by Equations 5 and 6, respectively. In the saturation regime, the drain current and transconductance are given by Equations 7 and 8, respectively.

$$g_d = \left. \frac{\partial I_d}{\partial V_d} \right|_{V_g = \text{const}} = \frac{Z}{L} \mu C_i (V_g - V_t) \quad (5)$$

$$g_m = \left. \frac{\partial I_d}{\partial V_g} \right|_{V_d = \text{const}} = \frac{Z}{L} \mu C_i V_d \quad (6)$$

$$I_{d,\text{sat}} = \frac{Z}{2L} \mu C_i (V_g - V_t)^2 \quad (7)$$

$$g_m = \frac{Z}{L} \mu C_i (V_g - V_t) \quad (8)$$

## 2.2. The MESFET

The principle of the MESFET is illustrated in Figure 1b. Here, the  $n^+$  source and drain are connected by an n-type region. The channel thickness is partially reduced by the depletion region that forms at the Schottky gate electrode, the thickness of which is controlled by the voltage applied to the gate. In a *normally off* device, the depletion region extends all over the n-type channel at zero gate voltage, whereas in a *normally on* MESFET, a portion of the channel is not depleted, thus ensuring the passage of a current at zero  $V_g$ .

To calculate the current–voltage characteristic, it is assumed that the conducting channel is neutral, that the space charge region is perfectly insulating, and that the boundary between the two regions is sharp. The drain current is obtained by integrating Equation 9, where  $N_d$  and  $d$  are the donor concentration and thickness of the n-channel, respectively, and  $W(x)$  the thickness of the space charge layer at point  $x$ . The latter is given by Equation 10, where  $V_{bi}$  is the built-in potential of the Schottky gate contact.

$$dV = I_d dR = I_d \frac{dx}{q\mu N_d Z [d - W(x)]} \quad (9)$$

$$W(x) = \sqrt{\frac{2\epsilon_s [V(x) + V_{bi} - V_g]}{qN_d}} \quad (10)$$

Inserting Equation 10 into Equation 9 and integrating from source to drain yields Equation 11, where  $g_0$ , given by Equation 12, is the conductance of the bulk n-type region, and  $V_p$  (Eq. 13) is the pinchoff voltage, that is, the gate voltage at which the depletion layer thickness is equal to that of the n-type channel.

$$I_d = g_0 \left\{ V_d - \frac{2 \left[ (V_d + V_{bi} - V_g)^{3/2} - (V_{bi} - V_g)^{3/2} \right]}{3V_p^{1/2}} \right\} \quad (11)$$

$$g_0 = q\mu N_d \frac{Zd}{L} \quad (12)$$

$$V_p = qN_d \frac{d^2}{2\epsilon_s} \quad (13)$$

As for the MISFET, Equation 11 is only valid for drain voltages such that the neutral channel extends up to the drain. For higher values of the drain voltage, saturation is reached and the drain current is given by Equation 14.

$$I_{d,sat} = g_0 \left[ \frac{V_p}{3} + \frac{2(V_{bi} - V_g)^{3/2}}{3V_p^{1/2}} - V_{bi} + V_g \right] \quad (14)$$

### 2.3. The Thin Film Transistor

The concept of the thin film transistor (TFT) was first introduced by Weimer in 1962.<sup>[13]</sup> This structure is well adapted to low conductivity materials, and is now currently used in amorphous silicon transistors.<sup>[8]</sup> As seen in Figure 1c, the source and drain electrodes form ohmic contacts directly to the conducting channel. Unlike both the structures described above, there is no depletion region to isolate the device from the substrate. Low off currents are only guaranteed by the low conductivity of the semiconductor. A second crucial difference to the MISFET is that, although the TFT is an insulated gate device, it operates in the *accumulation* regime and not in the inversion regime. For this reason, care has to be taken when transferring the equations of the drain current from the MISFET to the TFT. In fact, the absence of a depletion region leads to a simplification of Equation 2, which can now be written as Equation 15.

$$I_d = \frac{Z}{L} \mu C_i \left( V_g - V_t - \frac{V_d}{2} \right) V_d \quad (15)$$

Here, the threshold voltage is the gate voltage for which the channel conductance (at low drain voltages) is equal to that of the whole semiconducting layer. It is given by Equation 16, where  $N$  is the density of doping centers (donors or acceptors, depending on whether the semiconductor is n- or p-type). Equation 16 assumes that all doping centers are ionized, which is far from being the case in organic semiconductors, as will be seen later.

$$V_t = \frac{qNd}{C_i} \quad (16)$$

In the saturation regime, the current is given by Equation 7. Once again, it must be borne in mind that this equation was derived under assumptions that are not always fulfilled in organic semiconductors, particularly that of a constant mobility.

## 3. Charge Transport in Organic Materials

### 3.1. Hopping

In metals and conventional semiconductors, charge transport occurs in *delocalized* states, and is limited by the scattering of the carriers, mainly on phonons, that is, thermally induced lattice deformations. Such a model is no longer valid in low conductivity materials such as amorphous or organic semiconductors, where a simple estimate shows that the mean free path of carriers would become lower than the mean atomic distance. In these materials, transport occurs by hopping of charges between *localized* states. A main difference between the delocalized and localized transport is that, in the former, the transport is limited by phonon scattering, whereas in the latter, it is phonon assisted. Accordingly, the charge mobility decreases with temperature in conventional semiconductors, the reverse being true in most organic materials. Several models have been developed to rationalize the hopping transport. In most cases, the temperature dependence of the mobility follows a law of the form  $\mu = \mu_0 \exp[-(T_0/T)^{1/\alpha}]$ , where  $\alpha$  is an integer ranging from 1 to 4. The boundary between the localized and delocalized processes is usually taken at a mobility between 0.1 and 1 cm<sup>2</sup> V<sup>-1</sup> s<sup>-1</sup>. The mobility in highly ordered molecular crystals is close to that limit, so that there is still controversy as to whether the conductivity in these materials should be described by localized or delocalized transport.

### 3.2. The Small Polaron

Localization in conjugated organic materials occurs via the formation of *polarons*. A polaron results from the deformation of the conjugated chain under the action of the charge. In other words, in a conjugated molecule, a charge is self-trapped by the deformation it induces in the chain.

This mechanism of self-trapping is often described through the creation of localized states in the gap between the valence and the conduction bands, as shown in Figure 5 in the case of polythiophene.<sup>[14]</sup> The existence of such levels in doped conjugated polymers and oligomers has indeed been identified by UV-visible spectroscopy.

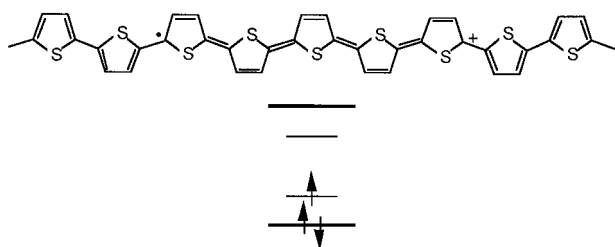


Fig. 5. A polaron in polythiophene. Top: Change in the chemical structure. Bottom: Corresponding energy diagram.

A useful model to describe the charge transport in organic materials is that of the small polaron, developed by Holstein.<sup>[15]</sup> It is a one-dimensional, one-electron model (that is, the electron–electron interactions are neglected). The total energy of the system is the sum of three terms. The lattice energy  $E_L$  (Eq. 17) is given by a sum of  $N$  harmonic oscillators that vibrate at a unique frequency  $\omega_0$ .

$$E_L = \sum_{n=1}^N \frac{1}{2M} \left( \hbar \frac{\partial}{\partial u_n} \right)^2 + \frac{1}{2} M \omega_0^2 u_n^2 \quad (17)$$

Here,  $u_n$  is the displacement of the  $n$ th molecule from its equilibrium position, and  $M$  the reduced mass of each molecular site. The electrons are described within the frame of the tight-binding approximation, where it is assumed that the effect of the potential at a given site of the one-dimensional chain is limited to its nearest neighbors. In that case, the energy dispersion of the electron is given by Equation 18, where  $J$  is the electron transfer energy and  $a$  the lattice constant. Finally, the electron–lattice coupling is accounted for by a term of the form given in Equation 19, where  $A$  is a constant.

$$E_k = E_0 - 2J \cos(ka) \quad (18)$$

$$\varepsilon_n = -A u_n \quad (19)$$

An important parameter is the polaron binding energy  $E_b$ , which is defined as the energy gain of an infinitely slow carrier due to the polarization and deformation of the lattice. In Holstein's model,  $E_b = A^2 / (2M\omega_0^2)$ . The limit of the small polaron turns up when the electronic bandwidth,  $2J$ , is small compared to the polaron binding energy. In that case, the electronic term of the total Hamiltonian can be treated as a perturbation. The mobility of the small polaron is calculated by solving the time-dependent Schrödinger equation. Its high-temperature limit ( $T > \Theta$ , where the Debye temperature  $\Theta$  is defined by  $k\Theta = \hbar\omega_0$ ) is given by Equation 20. It is worth pointing out that the term  $ea^2/\hbar$

has the dimension of a mobility, and is close to  $1 \text{ cm}^2 \text{ V}^{-1} \text{ s}^{-1}$  in most molecular crystals.

$$\mu = \sqrt{\frac{\pi}{2}} \frac{ea^2}{\hbar} \frac{J^2}{\sqrt{E_b}} (kT)^{-3/2} \exp\left(-\frac{E_b}{2kT}\right) \quad (20)$$

### 3.3. Field-Dependent Mobility

A general feature of charge transport in organic materials is that the mobility becomes field dependent at high electric field (namely, at fields in excess of  $\sim 10^5 \text{ V/cm}$ ).<sup>[16]</sup> This phenomenon occurs through a Poole–Frenkel mechanism,<sup>[17]</sup> in which the coulombic potential near the localized levels is modified by the applied field in such a way as to increase the tunnel transfer rate between sites. The general dependence of the mobility is given by Equation 21. Here,  $\mu(0)$  is the mobility at zero field,  $\beta = (e/\pi\epsilon\epsilon_0)^{1/2}$  the Poole–Frenkel factor, and  $F$  the magnitude of the electric field.

$$\mu(F) = \mu(0) \exp\left(\frac{q}{kT} \beta \sqrt{F}\right) \quad (21)$$

### 3.4. Multiple Trapping and Release

In the multiple trapping and release (MTR) model,<sup>[18]</sup> a narrow delocalized band is associated with a high concentration of localized levels that act as traps. During their transit through the delocalized levels, the charge carriers interact with the localized levels through trapping and thermal release. The following assumptions are usually made: First, the carriers arriving at a trap are instantaneously trapped with a probability close to one. Second, the release of trapped carriers is controlled by a thermally activated process. The resulting drift mobility  $\mu_D$  is related to the mobility  $\mu_0$  in the delocalized band by an expression of the form in Equation 22.

$$\mu_D = \mu_0 \alpha \exp\left(-\frac{E_t}{kT}\right) \quad (22)$$

In the case of a single trapping level,  $E_t$  corresponds to the distance between the trap level and the delocalized band edge, and  $\alpha$  is the ratio of the effective density of states at the delocalized band edge to the concentration of traps. In the case of energy-distributed traps, effective values of  $N_t$  and  $\alpha$  have to be calculated. The MTR model is currently the one most widely used to account for charge transport in amorphous silicon.

## 4. Fabrication Techniques

Conventional electronic devices are constructed on silicon wafers. The fabrication of a silicon MISFET starts with the diffusion (or implantation) of the source and drain, fol-

lowed by the growth of the insulating layer, usually thermally grown silicon oxide, and ends with the deposition of the electrodes. Organic semiconductors are obtained as thin films; accordingly, OFETs present an *inverted* architecture, in which the gate electrode is laid down first, the deposition of the semiconducting film usually being the last step. Most frequently, the gate is constituted by a highly doped silicon wafer, on which a silicon oxide layer is thermally grown. The source and drain are deposited on this insulating layer by conventional microlithographic techniques. The main advantage of this approach is the use of the standard technology of silicon microelectronics, and particularly that of microlithography, a well mastered procedure, which allows the fabrication of devices with small dimensions. One of its major drawbacks is that it is not compatible with an individual addressing of the various transistors constructed on the same substrate. However, other techniques that use organic substrates and insulators have been developed recently.

#### 4.1. Deposition of the Semiconducting Film

The deposition of the semiconductor is the determining step of the OFET fabrication, especially when one is using a thermally oxidized silicon wafer as substrate, where the rest of the process is controlled by conventional techniques.

##### 4.1.1. Electropolymerization

Electrochemical polymerization is one of the leading techniques for the synthesis of conducting polymers, and reports on electrochemically grown OFETs date back to the late 1980s.<sup>[6]</sup> Although the technique presents advantages in other applications of CPs, its drawbacks are numerous in the case of OFETs. First, electropolymerization only occurs on conducting substrates. For this reason, the semiconductor is first grown on the source and drain electrodes, its extension over the insulator being achieved by a lateral expansion of the deposit. This results in a highly disordered film, and a poor quality insulator–semiconductor interface. Second, the CP is obtained in its oxidized, conducting, form, and has to be reduced (generally electrochemically) in order to become semiconducting. This constitutes an additional source of disorder. Today, this technique is no longer used in the fabrication of OFETs.

##### 4.1.2. Solution-Processed Deposition

One of the most elegant ways to realize a nice polymer film is spin-coating. When the technique is well handled, it allows the production of very homogeneous films with perfect control of their thickness over relatively large areas. A requirement for this technique is a good solubility of the polymer. Unfortunately, a great number of CPs are not sol-

uble. The problem may be overcome either by grafting solubilizing groups to the polymer backbone,<sup>[19,20]</sup> or by the use of a soluble precursor polymer,<sup>[21,22]</sup> which is then converted to the CP by an appropriate physical or chemical treatment.

##### 4.1.3. Vacuum Evaporation

Spin-coating, which requires high viscosity solutions, is usually not applicable to small molecules. These are more appropriately deposited by vacuum evaporation, which consists of heating the material under reduced pressure. The process is conducted in a very high or ultra high vacuum chamber. The organic material is put into a metal boat, which is heated by Joule effects, or sometimes with an electron gun, and the substrate placed a few centimeters above the boat. We note that, in principle, this technique cannot be used for polymers, which tend to decompose by cracking at high temperatures. Its main advantages are the easy control of the thickness and purity of the film, and the fact that highly ordered films can be realized by monitoring the deposition rate and the temperature of the substrate. Its primary drawback is that it requires sophisticated instrumentation, in contrast to the simplicity and low cost of spin-coating.

##### 4.1.4. Langmuir–Blodgett Technique

An alternative means to make well-organized thin films of small molecules is the Langmuir–Blodgett (LB) technique, which allows fine control of both the structure and thickness of the film. We note, however, that this technique is in principle restricted to amphiphilic molecules, composed of a hydrophobic chain and a hydrophobic head-group, which is not the case for most molecules used in OFETs. Nevertheless, LB-grown OFETs have been reported with mixed layers of quinquethiophene (5T) and arachidic acid,<sup>[23]</sup> which gave well-behaved devices. However, the mixing of electrically active and inactive compounds leads to a substantial decrease of the mobility, as compared to that of a vacuum evaporated film.

#### 4.2. Substrate and Insulator

As mentioned above, most of the OFETs reported to date were constructed on a silicon wafer and used silicon oxide as the insulator. Such a structure does not take advantage of one of the main reasons for interest in organic materials, namely, the possibility of building electronic devices on plastic substrates. A second important drawback of the silicon-based structure is the impossibility of addressing individually the gates of transistors built on the same wafer, which prevents the realization of integrated circuits.

Several attempts have been made to build OFETs on plastic substrates. One of the first was reported by a group

at the Laboratoire des Matériaux Moléculaires of CNRS. The device was first built on a glass substrate, and used a spin-coated organic polymer as the insulator.<sup>[24]</sup> The glass substrate was then changed to a polymeric film (polyimide),<sup>[25]</sup> thus making the first “nearly all” organic transistor (the only non-organic materials being the metals used for the electrodes.) It is worth noting that these devices exhibited characteristics comparable to those made on silicon or glass, and that no noticeable loss of performance was observed upon bending the flexible substrate. However, in these devices the organic semiconductor and metal electrodes were still deposited by vacuum evaporation. More recently, Garnier et al. realized an OFET made by a printing technique,<sup>[26]</sup> again on a polymeric substrate. In fact, only the electrodes were really printed. A further step has been taken by a group at Bell Labs,<sup>[27]</sup> who built an all-printed device on an ITO-coated polyester substrate; all the subsequent layers, namely the polyimide insulator, semiconducting poly(3-alkylthiophene), and finally the source and drain, made of a conducting ink, were printed through stainless steel masks. Interestingly, all the components used in that OFET are commercially available.

## 5. Performance

Since the first report in 1987,<sup>[6]</sup> the performance of OFETs has continuously improved. The last two or three years have seen real breakthroughs, and OFETs can now compete with other thin film transistors such as amorphous silicon devices. The improvements mainly came from the possibility of making highly ordered films, and are therefore more significant for small molecules than for polymers. In this review, I shall restrict myself to the most recent results, and concentrate on two parameters that are of primary importance in OFETs, namely the field-effect mobility and the on-off current ratio. The latter indicates the ability of a device to shut down, and is particularly relevant in applications such as matrix active displays and logic circuits. On-off ratios of MOSFETs are in the  $10^9$  range, whereas those of a-Si:H TFT are limited to  $10^6$ . We note that a high mobility insures a high on current, and hence also contributes to a high on-off ratio.

### 5.1. Oligothiophenes

The chemical scheme of oligothiophenes ( $n$ T, where  $n$  stands for the number of thiophene units) is shown in Figure 6. Oligothiophenes used in OFETs are either non-substituted, or substituted at both ends by a linear alkyl group.

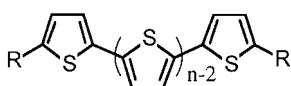


Fig. 6. Chemical structure of unsubstituted ( $R = H$ ) and alkyl end-substituted ( $R = C_nH_{2n+1}$ ) oligothiophenes.

The first report of a 6T-based OFET dates back to 1989.<sup>[28]</sup> This was also the first report of an OFET made with a small conjugated molecule. The importance of the ordering of the film first appeared when Waragai and Hotta showed that the dimethyl end-substitution of 3T to 5T leads to a 10 to 100 times increase of the mobility, as compared to their unsubstituted counterparts.<sup>[29]</sup> This was confirmed soon after in Thiais with dihexyl-substituted 6T (DH6T).<sup>[30]</sup> X-ray diffraction measurements on the latter compound showed that the improvement was related to the very regular arrangement of the film, which was formed of a regular superposition of layers, in each of which the molecules are packed parallel to each other and nearly perpendicular to the plane of the film. Such an arrangement is preserved over thicknesses of up to several micrometers, and makes the film a two-dimensional medium, in which the charge transport is favored in the direction parallel to the film, and hence perpendicular to the long axis of the molecules. Such an interpretation was confirmed when highly ordered films of the unsubstituted 6T were grown by heating the substrate and using low deposition rates,<sup>[31]</sup> which resulted in both a molecular packing and a field-effect mobility similar to that of DH6T. Identical results have been reported more recently by the Bell Labs group for both 6T<sup>[32]</sup> and DH6T.<sup>[33]</sup> Interestingly, the devices of the Bell Labs group were built on silicon wafers, whereas ours used a polymeric gate insulator, namely polymethylmethacrylate (PMMA). In a very recent report,<sup>[34]</sup> a group at IBM has measured mobility values for DH6T ranging from  $0.095$  to  $0.13 \text{ cm}^2 \text{ V}^{-1} \text{ s}^{-1}$  by using a parylene-c as the gate insulator. With a polyimide gate insulator, the mobility ranges from  $0.09$  to  $0.10 \text{ cm}^2 \text{ V}^{-1} \text{ s}^{-1}$ , whereas with PMMA it extends from  $0.04$  to  $0.08 \text{ cm}^2 \text{ V}^{-1} \text{ s}^{-1}$ , which compares well with that reported by the Thiais group.

A second significant feature found recently is that, in contrast with earlier reports, oligothiophenes of different lengths (from 4T to 8T) have practically identical field-effect mobility.<sup>[35–37]</sup> Representative data are gathered in

Table 1. Typical mobility [ $\text{cm}^2 \text{ V}^{-1} \text{ s}^{-1}$ ] of recent oligothiophene-based OFETs.

Compound	Unsubstituted	Dihexyl-substituted	Reference
4T	$10^{-4} - 6 \times 10^{-3}$		[35,36]
5T	$1.5 \times 10^{-3}$		[36]
6T	0.01 – 0.03	0.04 – 0.06	[30–32]
		0.09 – 0.13	[34]
8T	0.01 – 0.03	0.01	[35,37]

Table 1. It can also be noted that the mobility is practically independent of the presence or absence of alkyl end substitution. The poorer performance of short chains reported earlier has been attributed to problems of charge injection from the source and drain electrodes. This was confirmed by inserting a buffer layer of tetracyanoquinodimethane (TCNQ) between the 4T layer and the gold source and drain,<sup>[36]</sup> which leads to an enhanced drain current.

6T single crystals of macroscopic size have been grown recently in Thiais.<sup>[38]</sup> The mobility of OFETs built on these crystals (with a PMMA gate insulator) lies around  $0.1 \text{ cm}^2 \text{ V}^{-1} \text{ s}^{-1}$ .<sup>[39,40]</sup> Although this value is significantly higher than that obtained on polycrystalline 6T ( $0.02 \text{ cm}^2 \text{ V}^{-1} \text{ s}^{-1}$ ) and DH6T ( $0.05 \text{ cm}^2 \text{ V}^{-1} \text{ s}^{-1}$ ), the magnitude of the enhancement does not correspond to what would be expected if the mobility in polycrystalline films was limited only by grain boundaries. (As a comparison, the mobility of polycrystalline silicon is almost one hundred times lower than that of the single-crystalline material.) It is therefore of primary interest to determine whether the field-effect mobility in single crystalline 6T OFETs is limited only by flaws in the device (such as highly resistant contacts, or poor insulator–semiconductor interface) or indeed represents the upper limit in this material. In particular, the field-effect mobility of 6T crystals is still significantly lower than the time-of-flight mobility reported in anthracene<sup>[41]</sup> and other molecular crystals. We finally note that an alternative crystal structure has been identified by the Bell Labs group on melt-grown 6T crystals.<sup>[42]</sup> The polymorphism in oligothiophenes has been very recently confirmed in 4T.<sup>[43,44]</sup> Figure 7 shows a view along the unique axis of the crystal of the low temperature (LT) and high temperature (HT) forms of 4T. It will of course be of great interest to know whether the HT form has better charge transport properties than the LT form.

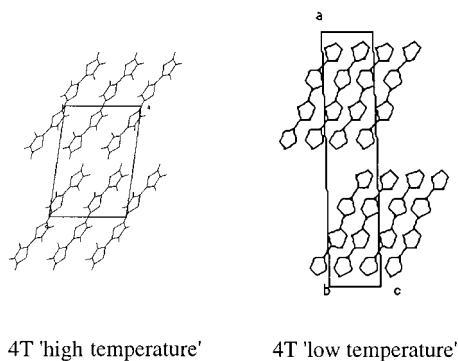


Fig. 7. View along the unique axis (b) of the two polymorphs of quaterthiophene (4T). Left: Low temperature (LT) form. Right: High temperature (HT) form.

## 5.2. Other Small Molecules

### 5.2.1. Phthalocyanines

Phthalocyanines (Pcs) were probably the first reported organic semiconductors,<sup>[7]</sup> and the ones that have been studied the most. They are thermally stable up to  $400^\circ\text{C}$ , and easy to evaporate under vacuum. The Pc molecule, shown in Figure 8, has the structure of a molecular cage, into which various metals can be introduced. The field effect was reported in a Pc as early as 1970<sup>[3]</sup> and OFETs were made in 1988.<sup>[45]</sup> Their field-effect mobility ranges between  $0.0001$  and  $0.01 \text{ cm}^2 \text{ V}^{-1} \text{ s}^{-1}$ .<sup>[45-47]</sup> Although Pcs have

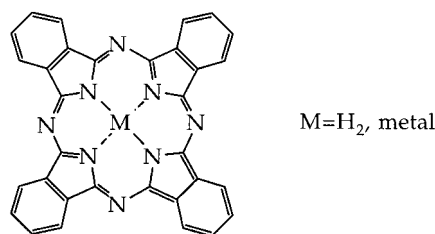


Fig. 8. Chemical structure of phthalocyanine (Pc). In metal Pcs, the central hydrogen atom is changed to the metal atom.

been reported to behave as both n- and p-type semiconductors, Pc-based OFETs are all p-type. The leading problem with Pcs remains their extreme sensitivity to oxygen.

### 5.2.2. Pentacene

Pentacene consists of five aligned condensed benzene rings. It belongs to the family of polyacenes, which were extensively studied as organic semiconductors during the 1960s and the 1970s. Although most of the pentacene-based OFETs consist of vacuum-evaporated films,<sup>[48-50]</sup> there have been reports on a solution-processed device,<sup>[51]</sup> using a soluble precursor molecule. Pentacene films have also been obtained by pulsed laser deposition,<sup>[52]</sup> a technique that is widely used in the field of high  $T_c$  superconductors, and which presents advantages in terms of speed of deposition and acceptable ranges of pressure. Table 2 sketches typ-

Table 2. Field-effect mobility [ $\text{cm}^2 \text{ V}^{-1} \text{ s}^{-1}$ ] of pentacene with various modes of deposition and substrate temperature (RT: room temperature).

Deposition mode	Substrate temperature [ $^\circ\text{C}$ ]	Mobility	Reference
Vacuum evaporation	RT	0.002	[48]
Spin-coated precursor		0.001	[51]
Pulsed-laser	RT	0.03	[52]
Vacuum evaporation	RT	0.038	[49]
Vacuum evaporation	85	0.4	[53]
Vacuum evaporation	120	0.62	[50]

ical results obtained with these different deposition techniques. Mobility up to  $0.62 \text{ cm}^2 \text{ V}^{-1} \text{ s}^{-1}$  has been reported.<sup>[50]</sup> This has been attributed to a highly ordered morphology, close to that of a single crystal.<sup>[53]</sup> However, such a value is only obtained in very narrow ranges of the deposition parameters (there exists in particular an optimum substrate temperature below and above which the high mobility is not obtained), which seems to pose serious problems of reproducibility. The on–off ratio of pentacene OFETs was reported to reach  $10^8$ .<sup>[49]</sup> We note, however, that such a ratio was measured by swinging the gate voltage between  $-100$  and  $+100 \text{ V}$ , a range which is far from agreeing with those used in microelectronics.

### 5.2.3. Other Fused-Ring Molecules

Among the other p-type molecular semiconductors that have been studied, one of the most promising is a fused ring compound, benzodithiophene, formed by two thiophene

rings fused at opposite sides of a benzene ring. A dimer of benzodithiophene has been synthesized by the Bell Labs group,<sup>[54]</sup> which offers a mobility up to  $0.04 \text{ cm}^2 \text{ V}^{-1} \text{ s}^{-1}$ .

#### 5.2.4. n-Type Semiconductors

Most of the organic semiconductors investigated so far are p-type in their non-intentionally doped form. Attempts to dope them to n-type usually lead to ambiguous results, one of the main problems being the mobility of the dopants under the high local fields that reign in electronic devices. The development of organic light-emitting diodes has introduced the concept of hole and electron transporting materials, which seems more pertinent for organic semiconductors. This would mean that a given material is "intrinsically" p- or n-type, n-type and p-type materials being characterized by their high electron affinity and low ionization potential, respectively. Because an organic metal–semiconductor (Schottky) diode is always made of a thin organic film sandwiched between a low-workfunction material (e.g., aluminum or calcium) and a high-workfunction metal (gold or ITO), measuring its current–voltage characteristic cannot help in determining whether the semiconductor is n- or p-type; in all cases, the direct current corresponds to the polarization where the low-workfunction metal (cathode) is negatively biased. In the OFET, because the sign of the carriers in the conducting channel changes, the accumulation regime is set up for *positive* gate biases in an n-type semiconductor, and for *negative* biases for a p-type semiconductor. Hence, the OFET is a reliable tool for characterizing a semiconductor. Evidence of n-type conductivity has been reported for several materials, a list of which is given in Table 3. A ma-

Table 3. Field-effect mobility [ $\text{cm}^2 \text{ V}^{-1} \text{ s}^{-1}$ ] of n-type organic semiconductors.

Compound	Mobility	Reference
TCNQ [a]	$1.9 \times 10^{-5}$	[55]
C <sub>60</sub>	0.002 – 0.08	[56,57]
C <sub>60</sub> + TDAE [b]	0.3	[56]
C <sub>70</sub>	0.002	[58]
Perylene-diimide	$1.5 \times 10^{-5}$	[59]
NDTCA [c]	0.002	[60]
PDTCA [d]	$10^{-4}$	[60]

[a] TCNQ: tetracyanoquinodimethane. [b] TDAE: tetrakisdimethylaminoethylene. [c] NDTCA: naphthalene tetracarboxylic dianhydride. [d] PDTCA: perylene tetracarboxylic dianhydride.

major problem of n-type materials is their strong instability with respect to oxygen. This is exemplified by C<sub>60</sub>,<sup>[56,57]</sup> the mobility of which can be as high as  $0.08 \text{ cm}^2 \text{ V}^{-1} \text{ s}^{-1}$  in ultra high vacuum but falls by 4 or 5 orders of magnitude upon exposure to air.<sup>[56]</sup> This could be due to problems of contacts, as illustrated by the fact that modifying the surface of the source and drain electrodes with tetrakisdimethylaminoethylene (TDAE) leads to a substantial increase of the mobility.<sup>[56]</sup>

### 5.3. Polymers

The performance of polymers stands roughly one order of magnitude below that of the small molecules. This can be understood from the fact that solution-processed materials present a poorer ordering than evaporated small molecules. We note, however, that a mobility of  $0.01 \text{ cm}^2 \text{ V}^{-1} \text{ s}^{-1}$  has been reached recently with a soluble regioregular polythiophene.<sup>[27,61]</sup> An even higher mobility (over  $0.1 \text{ cm}^2 \text{ V}^{-1} \text{ s}^{-1}$ ) was reported for polythienylenevinylene in 1993,<sup>[22]</sup> but this result has not been reproduced since then. We note finally that poly(*para*-phenylenevinylene) (PPV), the most used CP in organic light-emitting diodes, presents a very low field-effect mobility,  $10^{-7} \text{ cm}^2 \text{ V}^{-1} \text{ s}^{-1}$ .<sup>[62]</sup>

Brown and co-workers<sup>[63]</sup> have shown that the mobility of soluble polythiophene can be increased by doping the polymer. However, this increase is accompanied by an equivalent increase of the conductivity. Consequently, the gain in mobility is obtained at the expense of the on–off ratio, which reduces the technological interest of the feature. This behavior was rationalized by using a variable-range hopping model, a feature that was fortified by the temperature dependence of the conductivity, which followed the  $\exp[-(T_0/T)^{1/4}]$  law predicted by Mott. The mobility–conductivity relationship can be described by a simple power law,  $\mu \propto \sigma^\delta$ , with  $\delta$  around 0.7. Interestingly, on drawing a log–log plot of their data together with other data taken from the literature, Brown et al. find a "universal" curve, valid for all disordered organic semiconductors.

## 6. Models

The development of microelectronics would not have been possible without modeling of silicon devices. The modeling of OFETs is currently hampered by several features. First, the charge transport in organic semiconductors is still not well understood. Although there is a general agreement that it occurs via hopping between localized states, the exact nature of these hops is still controversial. Second, there are great differences between the behavior of OFETs made from different compounds; for instance, polymers do not behave the same as small molecules. Furthermore, the mode of preparation of the device seems to strongly affect its final performance. Nevertheless, a few attempts have been made; they generally concern one family of materials, mainly the oligothiophenes and, to a lesser extent, pentacene.

### 6.1. Charge Transport

Since 1991, the Thiais group has developed a charge transport model based on the multiple trapping and release (MTR) model, which is commonly used in amorphous sil-

icon TFTs.<sup>[64,65]</sup> A prominent feature shared by amorphous silicon TFTs and OFETs is that the field-effect mobility is *gate bias dependent*. This can be understood by recalling that a TFT operates in the accumulation regime, which means that as the gate bias is increased, the Fermi level gradually approaches the nearest delocalized band edge (see Fig. 3a). In amorphous silicon, there exists near the delocalized bands an important density of localized levels, which act as traps for charge carriers.<sup>[8]</sup> At low gate bias, nearly all induced charges go to the localized levels, where their mobility is very low. With an increase of the gate voltage, the Fermi level approaches the delocalized band and more traps are filled, which leads to an increase of the concentration of mobile carriers in the delocalized levels. As a result, the effective mobility increases. We have used this model to rationalize the characteristics of 6T- and DH6T-based OFETs. The first problem was how to determine a gate-bias-dependent mobility. This is difficult when the mobility is estimated from the saturation current and Equation 7 because, since Equation 7 contains a threshold voltage  $V_t$ , the departure of the experimental data from the  $\sqrt{Id}$  versus  $V_g$  straight line at low gate biases can be attributed to either a lower mobility or to a subthreshold regime. Instead, we used Equation 6 at very low drain voltage. In that case, the mobility is simply obtained by differentiating the drain current as a function of the gate voltage. In all cases, we observed that  $\mu$  was indeed gate bias dependent. We also measured the temperature dependence of the mobility, and found that it was thermally activated, with a gate-bias-dependent activation energy. These results were used to estimate the energy profile of the density of localized states, and the “trap-free” mobility, that is, the mobility corresponding to a high gate bias, at which all traps are filled. Interestingly, we found a similar trap-free mobility in 6T and DH6T, despite the fact that the effective mobility of the former is ten times lower than that of the latter. However, the magnitude of this trap-free mobility, namely  $0.04 \text{ cm}^2 \text{ V}^{-1} \text{ s}^{-1}$ , was still too low to correspond to transport in delocalized states, and a model based on the MTR model is probably not fully justified in our case.

More recently, a similar behavior has been reported in pentacene by Brown and co-workers.<sup>[66]</sup> They also used the transconductance (Eq. 6) at low drain voltage to calculate the mobility, and found a gate bias dependence of both the mobility and its activation energy. This was interpreted in the frame of a polaronic hopping transport, so that the activation energy was identified as the polaron binding energy. (We note that, according to Holstein's theory, Equation 20, the activation energy should rather correspond to *half* the polaron energy.) Once more, the variation of the activation energy is attributed to disorder, which induces deep localized levels. These levels are the first to be occupied at low gate bias. Increasing the gate bias moves the Fermi level to the polaronic levels, which are those seen at high gate voltages. For pentacene, this limit is around 0.1 eV (which would give a polaron binding energy of ~0.2 eV.) Finally, a

connection is made between the behavior of pentacene and that observed previously for doped polythiophene, where charge transport occurs through variable range hopping. According to Brown, the latter regime pertains to “highly” doped ( $N > 10^{18} \text{ cm}^{-3}$ ) materials, whereas the regime observed in pentacene is characteristic of low doping levels.

The polaron model was also used by Hotta and Waragai<sup>[10,67]</sup> to analyze temperature-dependent results on methyl-substituted oligothiophenes. While their data did not cover a sufficient temperature range for a clear temperature dependence of the mobility to be discerned, they noticed that  $\mu$  presented a *drain* voltage dependence, which they attributed to the  $F^{1/2}$  dependence given by Equation 21. Accordingly, the temperature-dependent mobility could be fitted to a thermally activated law of the form  $\mu = \mu_0 \exp(-E_{\text{tot}}/kT)$ , where  $E_{\text{tot}} = E_b/2 - \beta\sqrt{F}$ . By extrapolating  $E_{\text{tot}}$  to zero electric field, they found a polaron binding energy of 0.24, 0.18, and 0.16 eV for 4T, 5T, and 6T, respectively. We note that these values are not very different from that reported by Brown for pentacene.<sup>[66]</sup> However, the drain-voltage-dependent mobility reported by Hotta and Waragai could also be attributed to the phenomenon of channel shortening, which will be dealt with in the next section.

The Bell Labs group has reported a significantly different behavior for 6T.<sup>[68]</sup> We note that they estimated the mobility from the saturation current, Equation 7, a method that does not give access to a possible gate voltage dependence. When the temperature is lowered, a decrease of the mobility is detected as well. The activation energy corresponds to a binding energy of 0.1 eV, in reasonable agreement with previous reports. The remarkable point is that at temperatures lower than ~50 K, they observe a dramatic *rise* of the mobility, which then stabilizes to a value close to that measured at room temperature. The sharp transition is interpreted within Holstein's polaron model, and would mark the passing from the hopping regime, at high temperature, to the band regime, at low temperature. If this were correct, it would be the first evidence for the small polaron band regime. However, we note that, because of the very low value of the polaron bandwidth (less than  $10^{-4}$  eV for a typical organic crystal<sup>[15]</sup>), delocalized transport in such a band is unlikely in polycrystalline materials, where crystal defects are abundant. Obviously, this phenomenon would deserve further confirmation, and particularly measurements by methods other than the field effect.

## 6.2. Current–Voltage Characteristics

Attempts to model the current–voltage characteristics of OFETs are still scarce, but this article would not be complete without a short review of that field.

A preliminary model has been developed by the Thiais group, based on the above treated MTR model.<sup>[64]</sup> It rested

on two crude assumptions: First, a single trap level close to the valence band edge, and second, a constant microscopic (trap free) mobility. The main result was that, depending on the gate voltage, the drain current exhibits two regimes, namely, a trap-limited current at low gate bias, and a trap-free regime at high gate bias. The transition is marked by a change of the slope of the square root of the saturation drain current versus gate voltage plot. Accordingly, we defined a pseudo-threshold voltage at this transition, which explained the high value of the threshold voltage reported for early OFETs.

A different model has been reported by the Bell Labs group.<sup>[69]</sup> They assumed constant mobility and trap-free materials, but introduced two interesting improvements. First, they took into account the finite resistance of the source and drain electrode, and leakage through the insulating layer. More interestingly, they also tried to rationalize two effects induced by the use of a short channel. First, the so-called channel shortening that occurs when the channel length is comparable to the source and drain depletion layer width, in which case the gradual channel approximation is no longer valid.<sup>[70]</sup> In that case, the channel of length  $L$  is replaced by a channel of length  $L_1 = L - \Delta L$  in series with an insulating region of length  $\Delta L$ , with  $\Delta L = 0$  when  $V_d < V_{d,sat}$  and  $\Delta L \propto V_{d,sat} - V_d$  when  $V_d > V_{d,sat}$ . Here,  $V_{d,sat}$  is the drain saturation voltage. The effect of channel shortening is a slow increase of the drain current in the saturation regime, a feature that could account for the behavior reported by Hotta and Waragai of dimethyl-oligothiophenes.<sup>[67]</sup> The second short channel effect concerns a field-dependence mobility, which occurs for source–drain fields above  $10^5$  V/cm, in agreement with similar phenomena observed in other organic materials.

More recently, models have been developed to account for the on–off ratio of OFETs. We have shown that the accumulation regime was not sufficient to describe completely the operating mode of OFETs;<sup>[71]</sup> we have also to consider the depletion mode, which occurs when the sign of the gate voltage is reversed. Evidence for a depletion regime, which becomes important when the semiconductor has a significant doping level, can be seen in Figure 9. At zero gate voltage, a non-zero drain current flows, which can be reduced by applying a positive gate bias (in the case of a p-type material). The principle of the depletion regime is quite similar to that of the MESFET, with the difference that, unlike the MESFET, the TFT is an insulated gate device. Accordingly, Equation 10 changes to Equation 23.

$$W(x) = \frac{\epsilon_s}{C_i} \left[ \sqrt{1 + \frac{2C_i^2 (V_g - V_{fb} + V(x))}{qN\epsilon_s}} - 1 \right] \quad (23)$$

Here,  $V_{fb}$  is the flat-band potential, which accounts for the non-ideality of the MIS junction, and  $N$  the concentration of dopants (donor or acceptor, depending on whether

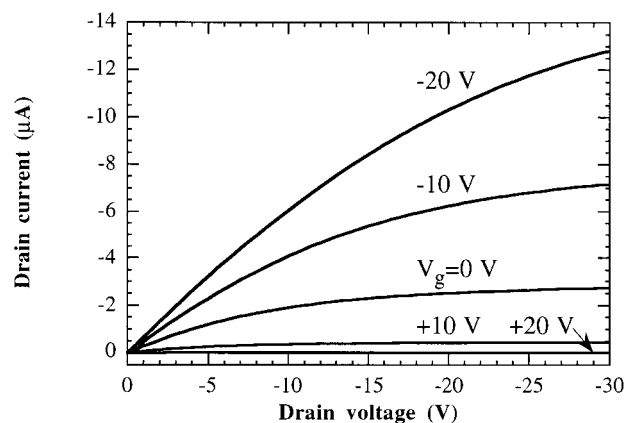


Fig. 9. Drain-current–voltage characteristic of a DH6T-based OFET, showing both an accumulation ( $V_g < 0$ ) and a depletion ( $V_g > 0$ ) regime.

the semiconductor is n- or p-type.) The drain current is now obtained by integrating Equation 9. We note, however, that in Equation 9, the concentration of carriers is assumed to equal the donor concentration  $N_d$ , as is usually done in inorganic semiconductor. In the Thiais group's model,<sup>[40,72]</sup> a distinction is introduced between the doping level  $N$  and the carrier density  $n$ . In the simplest case where the dielectric capacitance  $C_s = \epsilon_s/d$  is greater than  $C_i$ , which is the case in OFETs where the semiconducting film is thinner than the insulating layer, the drain current in the linear and saturation regimes is given by Equations 24 and 25, with the pinchoff voltage being given by Equation 26.

$$I_d = \frac{Z}{L} \mu \frac{n}{N} C_i (V_p - V_g) V_d \quad (24)$$

$$I_{d,sat} = \frac{Z}{2L} \mu \frac{n}{N} C_i (V_p - V_g)^2 \quad (25)$$

$$V_p = \frac{qNd^2}{2\epsilon_s} \left( 1 + 2 \frac{C_s}{C_i} \right) + V_{fb} \approx \frac{qNd}{C_i} + V_{fb} \quad (26)$$

If we assume that the mobility is the same in the depletion and the accumulation regime, a difference between  $n$  and  $N$  can be attributed to traps induced by disorder. Interestingly, we find that  $n/N$  ranges between  $10^{-2}$  and  $10^{-3}$  in 6T,<sup>[71,72]</sup> whereas it is close to unity in DH6T.<sup>[72]</sup> Once more, this could mirror the much better ordering of the latter compound. We also see from Equation 26 that an improvement of the on–off ratio can be obtained by reducing the pinchoff voltage, which can be done by lowering both the thickness of the semiconducting film and its doping level.

A difference between  $n$  and  $N$  has also been reported by Brown and co-workers,<sup>[63,66]</sup> who attribute it to a distribution of states below the Fermi level. The ratio  $n/N$  is found to vary from 0.01 in a disordered polymer (a derivative of polythiophene), to 0.25 in ordered pentacene. These authors have also developed a model to estimate the on–off ratio of their OFETs.<sup>[66]</sup> They defined two limiting

cases, depending on the doping level of the semiconductor. At high doping level, the on-off ratio is given by Equation 27, whereas at low doping level Equation 28 holds.

$$\frac{I_{\text{on}}}{I_{\text{off}}} = 1 + \frac{\mu C_i V_d}{\sigma 2d} \quad (27)$$

$$\frac{I_{\text{on}}}{I_{\text{off}}} = \frac{\mu C_i^2 V_d^2}{\sigma q N_a d^2} \quad (28)$$

Clearly, the on-off ratio is not solely dependent on the ratio of mobility to conductivity. It can also be enhanced by using an insulator with high capacitance per unit area, and also by lowering the thickness and doping level of the semiconductor layer.

## 7. Conclusions

The performance of OFETs has undergone real improvements during the past three years. These devices now compete with inorganic TFTs in terms of field-effect mobility, and it may reasonably be hoped that this will soon also be the case in terms of on-off ratio. We would like to stress two crucial needs for the development of organic FETs. First, because these devices are hampered by inherently limited performance, they will only compete if they can be fabricated with low cost technologies, such as spin-coating and printing techniques. We note that, from this standpoint, polymers present advantages over small molecules. Second, a considerable effort remains to be made to model the charge transport mechanisms in organic semiconductors. Such an effort should be directed both at theoretical work and to obtaining highly pure model materials. From this second viewpoint, small molecules are probably of more interest than polymers.

Received: October 24, 1997

[1] J. E. Lilienfeld, US Patent 1 745 175, **1930**.  
 [2] D. Kahng, M. M. Atalla, IRE Solid-State Devices Research Conference, Carnegie Institute of Technology, Pittsburgh, PA **1960**.  
 [3] D. F. Barbe, C. R. Westgate, *J. Phys. Chem. Solids* **1970**, *31*, 2679.  
 [4] M. L. Petrova, L. D. Rozenshtein, *Fiz. Tverd. Tela (Sov. Phys.—Solid State)* **1970**, *12*, 961.  
 [5] F. Ebisawa, T. Kurokawa, S. Nara, *J. Appl. Phys.* **1983**, *54*, 3255.  
 [6] H. Koezuka, A. Tsumura, T. Ando, *Synth. Met.* **1987**, *18*, 699; A. Tsumura, H. Koezuka, Y. Ando, *Synth. Met.* **1988**, *25*, 11.  
 [7] D. D. Eley, *Nature* **1948**, *162*, 819; D. D. Eley, G. D. Parfitt, M. J. Perry, D. H. Taysum, *Trans. Faraday Soc.* **1953**, *49*, 79.  
 [8] M. Shur, *Physics of Semiconductor Devices*, Prentice-Hall, Englewood Cliffs, NJ **1990**, pp. 437–446.  
 [9] G. Horowitz, *Adv. Mater.* **1990**, *2*, 287.  
 [10] S. Hotta, K. Waragai, *Adv. Mater.* **1993**, *5*, 896.  
 [11] H. E. Katz, *J. Mater. Chem.* **1997**, *7*, 369.  
 [12] S. M. Sze, *Physics of Semiconductor Devices*, 2nd ed., Wiley, New York **1981**.  
 [13] P. K. Weimer, *Proc. IRE* **1962**, *50*, 1462.  
 [14] W. R. Salaneck, S. Stafström, J. L. Brédas, *Conjugated Polymer Surfaces and Interfaces*, Cambridge University Press, Cambridge **1996**.  
 [15] T. Holstein, *Ann. Phys. (NY)* **1959**, *8*, 343.  
 [16] D. M. Pai, *J. Chem. Phys.* **1970**, *52*, 2285.  
 [17] J. Frenkel, *Phys. Rev.* **1938**, *54*, 647.  
 [18] P. G. Le Comber, W. E. Spear, *Phys. Rev. Lett.* **1970**, *25*, 509.

[19] Z. Xie, M. S. A. Abdou, X. Lu, M. J. Deen, S. Holdcroft, *Can. J. Phys.* **1992**, *70*, 1171.  
 [20] M. Willander, A. Assadi, C. Svensson, *Synth. Met.* **1993**, *57*, 4099.  
 [21] J. H. Burroughes, C. A. Jones, R. H. Friend, *Nature* **1988**, *335*, 137.  
 [22] J. H. Burroughes, R. H. Friend, P. C. Allen, *J. Phys. D, Appl. Phys.* **1989**, *22*, 956.  
 [23] H. Fuchigami, A. Tsumura, H. Koezuka, *Appl. Phys. Lett.* **1993**, *63*, 1372; H. Koezuka, H. Fuchigami, K. Hamano, A. Tsumura, T. Kurata, *Mol. Cryst. Liq. Cryst. Sci. Technol., Sect. A—Mol. Cryst. Liq. Cryst.* **1994**, *255*, 221.  
 [24] J. Paloheimo, P. Kuivalainen, H. Stubb, E. Vuorimaa, P. Yli-Lahti, *Appl. Phys. Lett.* **1990**, *56*, 1157.  
 [25] X. Z. Peng, G. Horowitz, D. Fichou, F. Garnier, *Appl. Phys. Lett.* **1990**, *57*, 2013.  
 [26] F. Garnier, G. Horowitz, X. Z. Peng, D. Fichou, *Adv. Mater.* **1990**, *2*, 592.  
 [27] F. Garnier, R. Hajlaoui, A. Yassar, P. Srivastava, *Science* **1994**, *265*, 1684.  
 [28] Z. Bao, Y. Feng, A. Dodabalapur, V. R. Raju, J. Lovinger, *Chem. Mater.* **1997**, *9*, 1299.  
 [29] G. Horowitz, D. Fichou, X. Z. Peng, Z. G. Xu, F. Garnier, *Solid State Commun.* **1989**, *72*, 381.  
 [30] H. Akimichi, K. Waragai, S. Hotta, H. Kano, H. Sakati, *Appl. Phys. Lett.* **1991**, *58*, 1500.  
 [31] F. Garnier, A. Yassar, R. Hajlaoui, G. Horowitz, F. Deloffre, B. Servet, S. Ries, P. Alnot, *J. Am. Chem. Soc.* **1993**, *115*, 8716.  
 [32] B. Servet, G. Horowitz, S. Ries, O. Lagorsse, P. Alnot, A. Yassar, F. Deloffre, P. Srivastava, R. Hajlaoui, P. Lang, F. Garnier, *Chem. Mater.* **1994**, *6*, 1809.  
 [33] A. Dodabalapur, L. Torsi, H. E. Katz, *Science* **1995**, *268*, 270; L. Torsi, A. Dodabalapur, A. J. Lovinger, H. E. Katz, R. Ruel, D. D. Davis, K. W. Baldwin, *Chem. Mater.* **1995**, *7*, 2247.  
 [34] H. E. Katz, A. Dodabalapur, L. Torsi, D. Elder, *Chem. Mater.* **1995**, *7*, 2238.  
 [35] C. D. Dimitrakopoulos, B. K. Furman, F. Graham, S. Hegde, S. Purushothaman, *Synth. Met.* **1998**, *92*, 47.  
 [36] H. E. Katz, L. Torsi, A. Dodabalapur, *Chem. Mater.* **1995**, *7*, 2235.  
 [37] R. Hajlaoui, D. Fichou, G. Horowitz, B. Nessakh, M. Constant, F. Garnier, *Adv. Mater.* **1997**, *9*, 557.  
 [38] R. Hajlaoui, G. Horowitz, F. Garnier, A. Arce-Brouchet, L. Laigre, A. Elkassmi, F. Demanze, F. Kouki, *Adv. Mater.* **1997**, *9*, 389.  
 [39] G. Horowitz, B. Bachet, A. Yassar, P. Lang, F. Demanze, J. L. Fave, F. Garnier, *Chem. Mater.* **1995**, *7*, 1337.  
 [40] G. Horowitz, F. Garnier, A. Yassar, R. Hajlaoui, F. Kouki, *Adv. Mater.* **1996**, *8*, 52.  
 [41] G. Horowitz, R. Hajlaoui and F. Kouki, *J. Phys. III (Paris)*, in press.  
 [42] N. Karl, J. Marktanner, R. Stehle, W. Warta, *Synth. Met.* **1991**, *42*, 2473.  
 [43] T. Siegrist, R. M. Fleming, R. C. Haddon, R. A. Laudise, A. J. Lovinger, H. E. Katz, P. Bridenbaugh, D. D. Davis, *J. Mater. Res.* **1995**, *10*, 2170.  
 [44] L. Antolini, G. Horowitz, F. Kouki, F. Garnier, *Adv. Mater.* **1998**, *10*, 382.  
 [45] T. Siegrist, C. Kloc, R. A. Laudise, H. E. Katz, R. C. Haddon, *Adv. Mater.*, **1998**, *10*, 379.  
 [46] R. Madru, G. Guillaud, M. Al Sadoun, M. Maitrot, J. J. André, J. Simon, R. Even, *Chem. Phys. Lett.* **1988**, *145*, 343.  
 [47] C. Clarisse, M. T. Riou, *J. Appl. Phys.* **1991**, *69*, 3324.  
 [48] Z. Bao, A. J. Lovinger, A. Dodabalapur, *Appl. Phys. Lett.* **1996**, *69*, 3066.  
 [49] G. Horowitz, X. Z. Peng, D. Fichou, F. Garnier, *J. Mol. Electron.* **1991**, *7*, 85.  
 [50] C. D. Dimitrakopoulos, A. R. Brown, A. Pomp, *J. Appl. Phys.* **1996**, *80*, 2501.  
 [51] D. J. Gundlach, Y. Y. Lin, T. N. Jackson, S. F. Nelson, D. G. Schlom, *IEEE Electron. Device Lett.* **1997**, *18*, 87.  
 [52] A. R. Brown, A. Pomp, C. M. Hart, D. M. Deleeuw, *Science* **1995**, *270*, 972; A. R. Brown, A. Pomp, D. M. de Leeuw, D. B. M. Klaassen, E. E. Havinga, P. Herwig, K. Müllen, *J. Appl. Phys.* **1996**, *79*, 2136.  
 [53] A. J. Salih, J. M. Marshall, J. M. Maud, *Phil. Mag. Lett.* **1997**, *75*, 169.  
 [54] J. G. Laquindanum, H. E. Katz, A. J. Lovinger, A. Dodabalapur, *Chem. Mater.* **1996**, *8*, 2542.  
 [55] J. G. Laquindanum, H. E. Katz, A. J. Lovinger, A. Dodabalapur, *Adv. Mater.* **1997**, *9*, 36.  
 [56] A. R. Brown, D. M. Deleeuw, E. J. Lous, E. E. Havinga, *Synth. Met.* **1994**, *66*, 257.  
 [57] R. C. Haddon, A. S. Perel, R. C. Morris, T. T. M. Palstra, A. F. Hebard, R. M. Fleming, *Appl. Phys. Lett.* **1995**, *67*, 121.

- [57] C. P. Jarrett, K. Pichler, R. Newbould, R. H. Friend, *Synth. Met.* **1996**, *77*, 35.
- [58] R. C. Haddon, *J. Am. Chem. Soc.* **1996**, *118*, 3041.
- [59] G. Horowitz, F. Kouki, P. Spearman, D. Fichou, C. Nogues, X. Pan, F. Garnier, *Adv. Mater.* **1996**, *8*, 242.
- [60] J. G. Laquindanum, H. E. Katz, A. Dodabalapur, A. J. Lovinger, *J. Am. Chem. Soc.* **1996**, *118*, 11331.
- [61] Z. Bao, A. Dodabalapur, A. J. Lovinger, *Appl. Phys. Lett.* **1996**, *69*, 4108.
- [62] K. Pichler, C. P. Jarrett, R. H. Friend, B. Ratier, A. Moliton, *J. Appl. Phys.* **1995**, *77*, 3523.
- [63] A. R. Brown, D. M. Deleeuw, E. E. Havinga, A. Pomp, *Synth. Met.* **1994**, *68*, 65.
- [64] G. Horowitz, P. Delannoy, *J. Appl. Phys.* **1991**, *70*, 469.
- [65] G. Horowitz, R. Hajlaoui, P. Delannoy, *J. Phys. III (Paris)* **1995**, *5*, 355.
- [66] A. R. Brown, C. P. Jarrett, D. M. de Leeuw, M. Matters, *Synth. Met.* **1997**, *88*, 37.
- [67] K. Waragai, H. Akimichi, S. Hotta, H. Kano, H. Sakaki, *Synth. Met.* **1993**, *57*, 4053.
- [68] L. Torsi, A. Dodabalapur, L. J. Rothberg, A. W. P. Fung, H. E. Katz, *Science* **1996**, *272*, 1462.
- [69] L. Torsi, A. Dodabalapur, H. E. Katz, *J. Appl. Phys.* **1995**, *78*, 1088.
- [70] M. Shur, M. Hack, J. G. Shaw, *J. Appl. Phys.* **1989**, *66*, 3371.
- [71] G. Horowitz, *Adv. Mater.* **1996**, *8*, 177.
- [72] G. Horowitz, F. Deloffre, F. Garnier, R. Hajlaoui, M. Hmyene, A. Yassar, *Synth. Met.* **1993**, *54*, 435.